INTERNATIONAL JOURNAL FOR NUMERICAL METHODS IN FLUIDS
Int. J. Numer. Meth. Fluids 2001; **36**: 441–464 (DOI: 10.1002/fld.139)

A stabilized incremental projection scheme for the incompressible Navier–Stokes equations

P. D. Minev*

Department of Mathematical Sciences, University of Alberta, Edmonton, Alberta, Canada

SUMMARY

It is well known that any spatial discretization of the saddle-point Stokes problem should satisfy the Ladyzhenskaya–Brezzi–Babuska (LBB) stability condition in order to prevent the appearance of spurious pressure modes. Particularly, if an equal-order approximation is applied, the Schur complement (or, as called some times, the Uzawa matrix) of the pressure system has a non-trivial null space that gives rise to such modes. An idea in the past was that all the schemes that solve a Poisson equation for the pressure rather than the Uzawa pressure equation (splitting/projection methods) should overcome this difficulty; this idea was wrong. There is numerical evidence that at least the so-called incremental projection scheme still suffers from spurious pressure oscillations if an equal-order approximation is applied. The present paper tries to distinguish which projection requires LBB-compliant approximation and which does not. Moreover, a stabilized version of the incremental projection scheme is derived. Proper bounds for the stabilization parameter are also given. The numerical results show that the stabilized scheme does indeed achieve second-order accuracy and does not produce spurious (node to node) pressure oscillations. Copyright © 2001 John Wiley & Sons, Ltd.

KEY WORDS: finite element method; pressure stabilization; projection methods

1. INTRODUCTION

The projection methods were introduced three decades ago with the pioneering studies of Chorin [1,2] and Temam [3]. Presently, they are one of the most popular methods for discretization of the unsteady incompressible Navier–Stokes equations. There are many peculiarities related to the performance of these methods, which were the subject of extensive research (for a recent review the reader is referred to Gresho and Sani [4]). Many of the properties of several such methods have been elucidated in a very interesting series of two papers of E and Liu [5,6]. They performed a normal modes analysis of the semi-discrete (in

* Correspondence to: Department of Mathematical Sciences, University of Alberta, 632 Central Academic Building, Edmonton, Alberta, Canada T6G 2G1.

Received 5 October 1999
Revised 25 August 2000

time only) Stokes equations employing the first-order Chorin's method and a second-order incremental (Bell *et al.* [7]) and non-incremental (Kim and Moin [8]) methods. It revealed that, since it is impossible to satisfy the exact boundary conditions for the pressure that follow from the semi-discrete equations, the pressure is polluted by either the formation of a spurious boundary layer around boundaries where Dirichlet boundary conditions are prescribed (Kim and Moin's method) or high-frequency oscillations, with a frequency of order $1/\Delta t$ (in case of the incremental method of Bell *et al.* [7]). They also proved some convergence results assuming a Ladyzhenskaya–Brezzi–Babuska (LBB)-compliant marker and cell (MAC) finite difference mesh.

In another series of papers, Guermond and Quartapelle [9–11] studied the properties of a slightly different incremental scheme employing a backward-difference scheme for temporal discretization and $P_2 - P_1$ triangular (and LBB-compliant) finite elements for spatial discretization. The same scheme combined with spectral element spatial discretization has also been used by Timmermans *et al.* [12]. Guermond and Quartapelle have provided convergence proofs for first- and second-order accurate schemes under the assumption that the finite elements satisfy the LBB stability condition. Their numerical results for a driven cavity flow undoubtedly showed that if an equal-order ($P_1 - P_1$) approximation is used, the pressure suffers from spurious oscillations, which do not disappear even after a much finer mesh is employed. The studies of Guermond and Quartapelle are the main source of inspiration for the present work. The author has used, with success, a very similar incremental projection scheme with $P_2 - P_1$ tetrahedra in three dimensions (see Minev and Ethier [13]) and recently obtained some controversial results while trying an equal-order ($P_2 - P_2$) approximation. On one hand, during the projection step (the evaluation of the pressure), the projection schemes solve a Laplace equation for the pressure. Thus, the null space of the discrete system for the pressure should be trivial (this is at least the naive thought about it). On the other hand, the pressure computed with some second-order projection schemes does suffer, in some particular situations, from spurious oscillations. The present study attempts to address this issue.

Another distinctive feature of the schemes aiming at the numerical solution of the Navier–Stokes equations is the way they treat the convective terms. Many of the schemes use some kind of explicit approximation (see Chorin [1], Temam [2], Timmermans *et al.* [12], Gresho *et al.* [14,15], Karniadakis *et al.* [16]) making the overall algorithm semi-implicit or explicit. Others use a semi-implicit approximation for the convective terms, making the algorithm unconditionally stable (see Bell *et al.* [7], Kim and Moin [8], Guermond and Quartapelle [11], van Kan [17]). The advantage of the former approach is that all the linear systems that need to be solved are symmetric and definite, and for such systems effective iterative solution methods exist. The advantage of the latter approach is its implicitness. The result from the momentum balance linear system, however, is non-symmetric and therefore the possibilities for an iterative solution are restricted. Moreover, this approach requires an update of the convective part of the matrix on each time step, which, at least for the three-dimensional case, is an expensive procedure. Since our solver is primarily aimed at three-dimensional problems we used the first approach throughout the present study. The convective terms are discretized explicitly using the method of characteristics (see Minev and Ethier [18]).

The remainder of the paper is organized as follows. The next section discusses the cause of instability of some of the projection/splitting[1] schemes and a possible way for a global stabilization. In Section 3 we discuss the bounds for the stabilization parameter of the scheme. Section 4 presents numerical results for a problem with an analytical solution and well-known benchmark flows. The main results of the present study are summarized in the last section.

2. SPLITTING/PROJECTION SCHEMES AND STABILIZATION

The Navier–Stokes equations (NSE) in primitive variables read

$$\frac{\partial \mathbf{u}}{\partial t} + (\mathbf{u}\cdot\nabla)\mathbf{u} = -\nabla p + \frac{1}{Re}\nabla^2\mathbf{u} \tag{1}$$

$$\nabla\cdot\mathbf{u} = 0 \tag{2}$$

For the sake of simplicity, in the present section we consider only Dirichlet boundary conditions of the type $\mathbf{u}|_{\partial\Omega} = \mathbf{d}$, Ω being the problem domain.

It is a very well-known fact that any attempt to solve these equations numerically meets two difficult problems. The first (and probably the easier) one is related to the discretization of the non-linear convection terms. The second one is related to the numerical treatment of the so-called saddle-point problem, which arises from the variational formulation obtained from Equations (1) and (2). After discretization, the linear system has the form

$$\begin{bmatrix} \mathbf{A} & \mathbf{L}^T \\ \mathbf{L} & 0 \end{bmatrix} \begin{bmatrix} \mathbf{u}_h \\ \mathbf{p}_h \end{bmatrix} = \begin{bmatrix} \mathbf{f}_h \\ \mathbf{g}_h \end{bmatrix} \tag{3}$$

where $\mathbf{A}$ is a linear combination of the mass, stiffness and eventually convection matrices and $\mathbf{L}$ is the discrete divergence. It is well known that the matrix of this system is indefinite and therefore its numerical solution is not straightforward.

2.1. Splitting schemes

One of the most effective and widely used approaches to circumvent the difficulties related to the two problems stated above is the 'divide and conquer' approach, which has different names under the different modifications: operator splitting, fractional step method, etc. The basic idea is to split the numerical treatment of the different operators (and unknowns) in the equations,

[1] The terms 'splitting scheme' and 'projection scheme' partially overlap. It is generally accepted to use 'projection scheme' if the scheme is based on a Helmholtz decomposition of the velocity, which usually requires that the pressure equation is solved after the convection–diffusion step. Those schemes can also be regarded as 'splitting' since the convection–diffusion part is split from the imposition of the incompressibility constraint. In the opposite case, 'splitting scheme' is a more appropriate term although an approximate projection step (solution of a separate pressure equation to enforce approximate incompressibility) is still performed.

thus solving the initially difficult problem in relatively easier sub-steps. There are numerous ways for such splitting and therefore a variety of different methods for solution of the unsteady NSE exist. As we shall see later, those methods are related in one way or another to probably the most classical approach for numerical solution of NSE—the so-called Uzawa method. It can be generalized as follows. Using an implicit or semi-implicit scheme, one discretizes the momentum equations (different spatial discretizations can be used). The incompressibility constraint must always be treated implicitly and as a result one obtains a system of type Equation (3). The algorithm then proceeds by solving a system for the pressure based on the so-called Schur complement matrix

$$\mathbf{L}\mathbf{A}^{-1}\mathbf{L}^T\mathbf{p}_h = -\mathbf{L}\mathbf{A}^{-1}\mathbf{f}_h + \mathbf{g}_h \tag{4}$$

and then substituting the so-computed pressure back into the momentum equations to solve for the velocity $\mathbf{u}_h$. Usually this approach is combined with an iterative solver for the resulting linear systems and therefore ends up with two nested iterative loops, which makes it quite expensive computationally although being very accurate. The most popular way to eliminate the nested iterative loops is to split the convection–diffusion part of the NSE from the incompressibility constraint which is usually imposed via a Poisson equation for the pressure (or pressure increment over the current time step). The convection–diffusion part can be further split into convection and diffusion sub-problems (Timmermans *et al.* [12], Karniadakis *et al.* [16], Minev and Ethier [18]) or the convection and diffusion can be treated together (Guermond and Quartapelle [9–11], Gresho *et al.* [14]). Of interest to the present study are the following two formulations (here we suppose that the velocities and pressures at levels t^{n-i}, $i = 0, \ldots, k$ are known and the task is to determine $\mathbf{u}^{n+1}$ and p^{n+1}).

Splitting 1 (incremental projection)

(i) Convection sub-step

$$\frac{\partial \tilde{\mathbf{u}}^{n-i}(s)}{\partial s} = -(\tilde{\mathbf{u}}^{n-i}(s)\cdot\nabla)\tilde{\mathbf{u}}^{n-i}(s), \quad 0 \le s \le (i+1)\Delta t, \quad i = 0, \ldots, k$$

$$\tilde{\mathbf{u}}^{n-i}(0) = \mathbf{u}^{n-i} \tag{5}$$

where $k = 0$ for a first-order scheme and $k = 1$ for a second-order scheme. This splitting of the convection from the rest of the equations can be derived using the general approach introduced by Maday *et al.* [19]. The velocities are marked by a tilde because they satisfy only the convective part of the equations. This pure convection equation can be solved by a variety of explicit methods, such as the Runge–Kutta (see Timmermans *et al.* [12]) or the method of characteristics, which is employed in the present study (see also Minev and Ethier [18]).

(ii) Diffusion sub-step

$$\tau_0\mathbf{u}_*^{n+1} + \tau_1\tilde{\mathbf{u}}^n + \tau_2\tilde{\mathbf{u}}^{n-1} = -\nabla p^n + \frac{1}{Re}\nabla^2\mathbf{u}_*^{n+1}$$

$$\mathbf{u}_*^{n+1} = \mathbf{d}^{n+1}$$

Here

$$\tau_0 = \frac{3}{2\Delta t}, \quad \tau_1 = -\frac{2}{\Delta t}, \quad \tau_2 = \frac{1}{2\Delta t}$$

for a second-order scheme and

$$\tau_0 = \frac{1}{\Delta t}, \quad \tau_1 = -\frac{2}{\Delta t}, \quad \tau_2 = 0$$

for a first-order scheme.

(iii) Incompressibility sub-step

$$\tau_0(\mathbf{u}^{n+1} - \mathbf{u}_*^{n+1}) + \nabla(p^{n+1} - p^n) = 0, \qquad \nabla\cdot\mathbf{u}^{n+1} = 0$$

$$\mathbf{n}\cdot\mathbf{u}|_{\partial\Omega}^{n+1} = \mathbf{n}\cdot\mathbf{d}^{n+1} \tag{6}$$

This sub-step is usually resolved by taking the divergence of the pressure equation and imposing the incompressibility constraint, which results in the pressure Poisson equation (PPE)

$$\tau_0\nabla\cdot\mathbf{u}_*^{n+1} = \nabla^2(p^{n+1} - p^n) \tag{7}$$

usually supplied with homogeneous Neumann boundary conditions.

If the convection is discretized semi-implicitly, (i) and (ii) can be unified, as done by Guermond and Quartapelle [9–11], into a convection–diffusion sub-step

$$\tau_0\mathbf{u}_*^{n+1} + \tau_1\mathbf{u}^n + \tau_2\mathbf{u}^{n-1} + [(\gamma_1\mathbf{u}_*^n + \gamma_2\mathbf{u}_*^{n-1})\cdot\nabla]\mathbf{u}_*^{n+1} = -\nabla p^n + \frac{1}{Re}\nabla^2\mathbf{u}_*^{n+1}$$

$$\mathbf{u}_*^{n+1} = \mathbf{d}^{n+1} \tag{8}$$

with $\gamma_1 = 1$, $\gamma_2 = 0$ for a first-order scheme and $\gamma_1 = 2$, $\gamma_2 = -1$ for a second-order scheme. Furthermore, the velocity $\mathbf{u}^{n-i}$, $i = 0, 1$ can be substituted from (iii) and the final momentum equation takes the form

$$\tau_0\mathbf{u}_*^{n+1} + \tau_1\mathbf{u}_*^n + \tau_2\mathbf{u}_*^{n-1} + [(\gamma_1\mathbf{u}_*^n + \gamma_2\mathbf{u}_*^{n-1})\cdot\nabla]\mathbf{u}_*^{n+1} =$$
$$-\nabla(\delta_1 p^n + \delta_2 p^{n-1} + \delta_3 p^{n-2}) + \frac{1}{Re}\nabla^2\mathbf{u}_*^{n+1} \tag{9}$$

where $\delta_1 = 2$, $\delta_2 = -1$, $\delta_3 = 0$ in case of a first-order scheme and $\delta_1 = 7/3$, $\delta_2 = -5/3$, $\delta_3 = 1/3$ in case of a second-order scheme. Then, $\mathbf{u}_*^{n+1}$ is admitted as an approximation to $\mathbf{u}^{n+1}$ and the velocity is not corrected on incompressibility sub-step (iii). This momentum equation is used

by Guermond and Quartapelle [9–11] to formulate first- and second-order incremental schemes. These schemes are equivalent to the ones defined by (i)–(iii) if applied to the unsteady Stokes equations. Otherwise they require the solution of a non-symmetric system on the convection–diffusion step. In the case of a finite element spatial discretization, *Splitting 1* requires solving two symmetric systems in order to compute the velocity $\mathbf{u}^{n+1}$ rather then one non-symmetric, as required by the scheme of Guermond and Quartapelle. The latter scheme is also unconditionally stable compared with the conditionally stable method of characteristics. The numerical experiments, however, show that its stability restriction is relatively weak and (for a wide variety of problems) the time step is rather restricted for reasons of accuracy. Moreover, the Guermond and Quartapelle approach requires the computation of the convection matrix at each time step, which, at least in the three-dimensional case, is an expensive procedure. Therefore we chose the scheme in (i)–(iii). The consistent mass matrix in step (iii) can be exchanged with a lumped version as done by Gresho *et al.* [14,15], but even the consistent matrix usually takes very few iterations to invert compared with the momentum and pressure solvers.

Splitting 2:

(i) Convection sub-step: the same as in (i) of *Splitting 1.*

(ii) Incompressibility sub-step

$$\tau_0\mathbf{u}_*^{n+1} + \tau_1\tilde{\mathbf{u}}^n + \tau_2\tilde{\mathbf{u}}^{n-1} = -\nabla p^{n+1}, \qquad \nabla\cdot\mathbf{u}_*^{n+1} = 0 \tag{10}$$

(iii) Diffusion sub-step

$$\tau_0\mathbf{u}^{n+1} + \tau_1\tilde{\mathbf{u}}^n + \tau_2\tilde{\mathbf{u}}^{n-1} = -\nabla p^{n+1} + \frac{1}{Re}\nabla^2\mathbf{u}^{n+1}$$

$$\mathbf{u}^{n+1} = \mathbf{d}^{n+1} \tag{11}$$

Note that if we subtract the first equation of (10) from (11) we obtain

$$\tau_0\mathbf{u}^{n+1} - \tau_0\mathbf{u}_*^{n+1} = \frac{1}{Re}\nabla^2\mathbf{u}^{n+1} \tag{12}$$

In the case of a first-order scheme ($\tau_0 = 1/\Delta t,\ \tau_1 = -1/\Delta t,\ \tau_2 = 0$) and if the convection is discretized by a Euler explicit scheme (or in the case of unsteady Stokes equations), this formulation becomes equivalent to the first-order accurate version of the splitting scheme proposed by Karniakakis *et al.* [16]. If we discretize the convection terms by means of a higher-order Adams–Bashforth and the diffusion terms by means of a higher-order Adams–Moulton scheme, this analogy can be extended to higher-order schemes as well. As mentioned by those authors, it suffers from large splitting errors if a homogeneous Neumann condition on p^{n+1} is imposed. Therefore they proposed to use an extrapolation for the pressure boundary condition, which allows us to construct higher-order schemes.

The derivation of *Splitting 1* is discussed by Timmermans *et al.* [12] while the framework for derivation of *Splitting 2* is provided by Karniadakis *et al.* [16].

2.2. Equal-order approximation

So far, we have considered only the time discretization of the NSE leaving the choice of the spatial approximation of the velocity and pressure open. It is well known that system (3) has a unique solution for the velocity and pressure unknowns if the approximation spaces $\mathbf{V}_h$ for the velocity and P_h for the pressure are LBB compliant, i.e.

$$\exists \theta_s > 0, \quad \sup_{\mathbf{v} \in \mathbf{V}_h} \frac{\mathbf{L}(\mathbf{v}, q)}{\|\mathbf{v}\|_{\mathbf{V}_h}} \geq \theta_s \|q\|_{P_h}, \quad \forall q \in P_h \tag{13}$$

It is also well known that if $\mathbf{V}_h \equiv P_h$, the pressure solution may suffer from spurious oscillations. From a linear algebra point of view, the reason for these oscillations is the fact that the null space of the Schur complement is non-trivial. Since both *Splitting 1* and *Splitting 2* solve a Poisson equation for the pressure rather than inverting the Schur complement, one may think that these formulations avoid the LBB constraint. However, as correctly noticed by Guermond and Quartapelle [11], this is not true. Their numerical simulations of a driven cavity using a $P_1 - P_1$ approximation clearly show that the pressure contains spurious modes. They also essentially used the LBB constraint in the analysis of the error of their version of *Splitting 1*. However, it is not quite clear why the pressure is sometimes unstable if the LBB condition is not satisfied. A possible explanation is the following. Let us consider the unsteady Stokes equations and write the fully discrete system derived from Guermond and Quartapelle's version of *Splitting 1* as

$$\left(\tau_0 \mathbf{M} + \frac{1}{Re}\mathbf{S}\right)\mathbf{u}_{h,*}^{n+1} = -(\tau_1 \mathbf{M}\mathbf{u}_h^n + \tau_2 \mathbf{M}\mathbf{u}_h^{n-1}) + \mathbf{L}^T(\delta_0 \mathbf{p}_h^n + \delta_1 \mathbf{p}_h^{n-1} + \delta_2 \mathbf{p}_h^{n-1}) \tag{14}$$

$$\mathbf{S}_p(\mathbf{p}_h^{n+1} - \mathbf{p}_h^n) = -\tau_0 \mathbf{L}\mathbf{u}_{h,*}^{n+1} \tag{15}$$

with $\mathbf{M}$ and $\mathbf{S}$ being the mass and stiffness matrices for the velocity and $\mathbf{S}_p$ being the pressure stiffness matrix (with homogeneous Neumann boundary condition). The substitution of $\mathbf{u}_{h,*}^{n+1}$ from Equations (14) into (15) gives

$$\mathbf{S}_p(\mathbf{p}_h^{n+1} - \mathbf{p}_h^n) = -\tau_0 \mathbf{L}\mathbf{A}^{-1}[\mathbf{L}^T(\delta_0 \mathbf{p}_h^n + \delta_1 \mathbf{p}_h^{n-1} + \delta_2 \mathbf{p}_h^{n-2}) - (\tau_1 \mathbf{M}\mathbf{u}_h^n + \tau_2 \mathbf{M}\mathbf{u}_h^{n-1})] \tag{16}$$

where $\mathbf{A} = \tau_0 \mathbf{M} + 1/Re\mathbf{S}$. It is quite clear that this is just the first step of a preconditioned iteration for solving a system of type Equation (4), which follows from the unsteady Stokes equations. The initial guess is $\delta_0 \mathbf{p}_h^n + \delta_1 \mathbf{p}_h^{n-1} + \delta_2 \mathbf{p}_h^{n-2}$, the preconditioning matrix is $\mathbf{S}_p$ and the relaxation parameter is given by τ_0. It is also clear that if a steady state is achieved, then the time stepping becomes a preconditioned iterative procedure for inverting the Schur complement matrix, which follows from the steady Stokes equations, i.e. in such a case we attempt to

solve the uncoupled (steady) system (3) using an iterative procedure (Uzawa iteration). Subsequently, the LBB condition should be satisfied by the velocity–pressure approximation in order to guarantee the pressure stability. *Splitting 2* can be identified to be the first step of the same iterative process starting with a zero initial guess for the pressure. In the steady limit (for a Stokes flow) it will produce a constant pressure unless a more accurate than the homogeneous Neumann boundary condition for the pressure is used. The accuracy issues of this scheme are studied thoroughly by Orszag *et al.* [20].

We shall now try to shed some light on the prospects for stabilization of the incremental *Splitting 1*, taking into account the discussion above. Let us perform step (i) of both splitting algorithms above and discretize the NSE in time using a backward difference scheme to produce the following generalized Stokes problem (all the subsequent considerations are valid if a body force is included in the equations; we omit this term for the sake of simplicity):

$$\tau_0\mathbf{u}^{n+1} + \tau_1\tilde{\mathbf{u}}^n + \tau_2\tilde{\mathbf{u}}^{n-1} = -\nabla p^{n+1} + \frac{1}{Re}\nabla^2\mathbf{u}^{n+1}$$

$$\mathbf{u}^{n+1} = \mathbf{d}^{n+1}$$

$$\nabla\cdot\mathbf{u}^{n+1} = 0 \tag{17}$$

Its Galerkin formulation reads

Find

$$\mathbf{u}^{n+1}\in(H^1(\Omega))^3 \quad \textit{and} \quad p^{n+1}\in L_0^2(\Omega) = \left\{q\in L^2(\Omega):\ \int_\Omega q\ \mathrm{d}\Omega = 0\right\}$$

such that

$$(\mathbf{u}_\tau^{n+1}, \mathbf{v}) + \frac{1}{Re}(\nabla\mathbf{u}^{n+1}, \nabla\mathbf{v}) - (p^{n+1}, \nabla\cdot\mathbf{v}) = 0, \quad \forall\mathbf{v}\in(H_0^1(\Omega))^3$$

$$(\nabla\cdot\mathbf{u}^{n+1}, q) = 0, \quad \forall q\in L_0^2(\Omega)$$

$$\mathbf{u}^{n+1} = \mathbf{d}^{n+1} \quad \text{on } \partial\Omega \tag{18}$$

where $\mathbf{u}_\tau^{n+1} = \tau_0\mathbf{u}^{n+1} + \tau_1\tilde{\mathbf{u}}^n + \tau_2\tilde{\mathbf{u}}^{n-1}$.

A classical way to stabilize the system is to add to the second equation of (18) the residual of the momentum equation in (17) multiplied by ∇q (more about this regularization approach can be found in Franca *et al.* [21] and Axelsson *et al.* [22]), weighted by a small positive parameter σ. Then the stabilized formulation reads

Find

$$\mathbf{u}^{n+1}\in(H^1(\Omega))^3 \quad \textit{and} \quad p^{n+1}\in L_0^2(\Omega)\cap H^1(\Omega)$$

such that

$$(\mathbf{u}_\tau^{n+1}, \mathbf{v}) + \frac{1}{Re}(\nabla \mathbf{u}^{n+1}, \nabla \mathbf{v}) - (p^{n+1}, \nabla \cdot \mathbf{v}) = 0, \quad \forall \mathbf{v} \in (H_0^1(\Omega))^3$$

$$(\nabla \cdot \mathbf{u}^{n+1}, q) + \sigma\left[(\mathbf{u}_\tau^{n+1}, \nabla q) - \frac{1}{Re}(\nabla^2 \mathbf{u}^{n+1}, \nabla q) + (\nabla p^{n+1}, \nabla q)\right] = 0, \quad \forall q \in H^1(\Omega) \cap L_0^2(\Omega)$$

$$\mathbf{u}^{n+1} = \mathbf{d}^{n+1} \quad \text{on } \partial\Omega \tag{19}$$

This formulation is clearly consistent with Equation (18) since the residual added to the incompressibility constraint turns to zero for the exact solution of the generalized Stokes problem. After integration by parts of the acceleration term $(\mathbf{u}_\tau^{n+1}, \nabla_q)$, Equation (19) becomes

$$(\nabla p^{n+1}, \nabla q) = -\left(\frac{1}{\sigma} - \tau_0\right)(\nabla \cdot \mathbf{u}^{n+1}, q) + (\nabla \cdot (\tau_1 \tilde{\mathbf{u}}^n + \tau_2 \tilde{\mathbf{u}}^{n-1}), q) - \int_{\partial\Omega} \mathbf{u}_\tau^{n+1} \cdot \mathbf{n} q \, \mathrm{d}s + \frac{1}{Re}(\nabla^2 \mathbf{u}^{n+1}, \nabla q) \tag{20}$$

where $\mathbf{n}$ is the unit outward normal to $\partial\Omega$. For $\sigma = 1/\tau_0$, Equation (20) is very similar to the Galerkin formulation of the pressure equation, which follows from sub-step (ii) of *Splitting 2* provided that a proper Neumann boundary condition for the pressure is used. Indeed, the last term in Equation (20) can be integrated by parts and then, applying the incompressibility

$$(\nabla p^{n+1}, \nabla q) = (\nabla \cdot (\tau_1 \tilde{\mathbf{u}}^n + \tau_2 \tilde{\mathbf{u}}^{n-1}), q) - \frac{1}{Re}(\nabla \cdot \nabla^2 \mathbf{u}^{n+1}, q) - \int_{\partial\Omega} \mathbf{u}_\tau^{n+1} \cdot \mathbf{n} q \, \mathrm{d}s + \frac{1}{Re} \int_{\partial\Omega} \nabla^2 \mathbf{u}^{n+1} \cdot \mathbf{n} q \, \mathrm{d}s \tag{21}$$

The surface integrals are exactly the contribution of the Neumann pressure boundary condition that follows from sub-step (iii) of *Splitting 2*. The difference comes from the term $1/Re(\nabla \cdot \nabla^2 \mathbf{u}^{n+1}, q)$. However, as discussed by Axelsson *et al.* [22], this term is usually very small (especially at large Reynolds numbers). Thus, *Splitting 2* supplied with a proper pressure boundary condition is expected to be stable if an equal-order approximation is used.[2] Unfortunately, this formulation is unusable since it couples the velocity and pressure at time level $n+1$. This difficulty can be circumvented in two ways. The first one is to use a high-order

[2] A similar conclusion can be drawn for all the non-incremental schemes, including the one proposed by Chorin and Temam. Of course, the issue of 'proper pressure boundary conditions' is quite non-trivial. The numerical experiments with homogeneous Neumann pressure boundary conditions and a non-incremental scheme with a $P_2 - P_2$ approximation did indeed yield non-oscillating pressure results in the case of a backward-facing step flow. However, the divergence of the steady velocity field was a few orders of magnitude higher than the one computed with a proper $P_2 - P_1$ approximation. For the same flow, the incremental projection scheme needed a stabilization (see Section 4).

extrapolation to the pressure boundary condition, as suggested by Karniadakis *et al.* [16]. The second one is to perform the defect-correction iteration suggested by Axelsson *et al.* [22]. In both cases, however, one needs to compute an approximation to the last term in Equation (21), which is not a trivial matter in case of the usual C^0 finite element interpolation and complex geometries. As it will be shown in Section 4, at large Reynolds numbers this term can be neglected and one can obtain reasonably accurate results. However, a more suitable (globally) stable formulation can be obtained following the idea of *Splitting 1*. As already mentioned, it can be considered as the first step of a preconditioned iteration for solution of the pressure equation

$$\mathbf{L}\mathbf{A}^{-1}\mathbf{L}^T\mathbf{p}_h = \mathbf{L}\mathbf{A}^{-1}(\tau_1\mathbf{M}\tilde{\mathbf{u}}_h^n + \tau_2\mathbf{M}\tilde{\mathbf{u}}_h^{n-1}) \tag{22}$$

The spatial discretization of the first equations of (19) and (20) using an equal-order approximation yields

$$\mathbf{A}\mathbf{u}_h^{n+1} = \mathbf{L}^T\mathbf{p}_h^{n+1} - (\tau_1\mathbf{M}\tilde{\mathbf{u}}_h^n + \tau_2\mathbf{M}\tilde{\mathbf{u}}_h^{n-1}) \tag{23}$$

$$\hat{\sigma}\mathbf{S}_p\mathbf{p}_h^{n+1} + \mathbf{L}\mathbf{u}_h^{n+1} = \hat{\sigma}\mathbf{L}(\tau_1\tilde{\mathbf{u}}_h^n + \tau_2\tilde{\mathbf{u}}_h^{n-1}) - \hat{\sigma}\mathbf{f}_s + \hat{\sigma}\mathbf{D}(\mathbf{u}_h^{n+1}) \tag{24}$$

where $\hat{\sigma} = (1/\sigma - \tau_0)^{-1}$, $\mathbf{f}_s$ is the contribution of the first surface integral in Equation (20) (known from the boundary conditions) and $\mathbf{D}(\mathbf{u}_h^{n+1})$ is some kind of approximation of the last term appearing in Equation (20). Since, as already mentioned, such an approximation is quite awkward to compute if a C^0 approximation is used, we neglect it in our further considerations, thus introducing an additional splitting error, which is controlled by the small parameter $\hat{\sigma}$. Substituting $\mathbf{u}^{n+1}$ from Equation (23) into Equation (24) yields the following equation for the pressure:

$$[\hat{\sigma}\mathbf{S}_p + \mathbf{L}\mathbf{A}^{-1}\mathbf{L}^T]\mathbf{p}_h^{n+1} = \hat{\sigma}\mathbf{L}(\tau_1\tilde{\mathbf{u}}_h^n + \tau_2\tilde{\mathbf{u}}_h^{n-1}) + \mathbf{L}\mathbf{A}^{-1}\mathbf{M}(\tau_1\tilde{\mathbf{u}}_h^n + \tau_2\tilde{\mathbf{u}}_h^{n-1}) - \hat{\sigma}\mathbf{f}_s \tag{25}$$

It is quite similar to Equation (22) except for the terms multiplied by the small parameter $\hat{\sigma}$. Now, following the idea that the incremental *Splitting 1* is actually a first step of a Richardson iteration for solving Equation (22) with a preconditioner given by $\mathbf{S}_p$ we can formulate the projection step of the stabilized formulation as the first step of an iteration for solving Equation (25) with a correspondingly adjusted preconditioner given by $(1 + \hat{\sigma}/\tau_0)\mathbf{S}_p$. The Galerkin formulation of the PPE then reads

$$(\nabla[(1+\hat{\hat{\sigma}})p^{n+1} - p^n], \nabla q) = -\tau_0(\nabla\cdot\mathbf{u}_*^{n+1}, q) + \hat{\hat{\sigma}}(\nabla\cdot(\tau_1\tilde{\mathbf{u}}^n + \tau_2\tilde{\mathbf{u}}^{n-1}), q) - \hat{\hat{\sigma}}\int_{\partial\Omega}\mathbf{u}_\tau^{n+1}\cdot\mathbf{n}q\,\mathrm{d}s \tag{26}$$

where $\hat{\hat{\sigma}} = \hat{\sigma}\tau_0$. The overall stabilized incremental projection scheme with the projection step written as a Poisson problem (and in case of the NSE) reads

Stabilized Incremental Projection

(i) Convection sub-step: the same as in (i) of *Splitting 1*.
(ii) Diffusion sub-step: the same as in (ii) of *Splitting 1*.
(iii) Incompressibility sub-step:
- Solve Equation (26) for p^{n+1}.
- Update the velocity according to

$$\tau_0(\mathbf{u}^{n+1} - \mathbf{u}_*^{n+1}) + \nabla(p^{n+1} - p^n) = 0$$

$$\mathbf{n}\cdot\mathbf{u}\big|_{\partial\Omega}^{n+1} = \mathbf{n}\cdot\mathbf{d}^{n+1} \tag{27}$$

Remark 1
Note that Equation (26) is a linear combination of the PPE's (more precisely their Galerkin formulations), which follow from the incompressibility sub-steps of *Splitting 1*, *Splitting 2*, Equations (6) and (10), with coefficients 1 and $\hat{\hat{\sigma}}$. One can do the same while updating the velocity and instead of Equation (27) use the linear combination of Equations (27) and (11) for this purpose

$$\tau_0(1+\hat{\hat{\sigma}})\mathbf{u}^{n+1} + \hat{\hat{\sigma}}(\tau_1\tilde{\mathbf{u}}^n + \tau_2\tilde{\mathbf{u}}^{n-1}) = -\nabla[(1+\hat{\hat{\sigma}})p^{n+1} - p^n] + \frac{\hat{\hat{\sigma}}}{Re}\nabla^2\mathbf{u}^{n+1} + \tau_0\mathbf{u}_*^{n+1}$$

$$\mathbf{u}^{n+1} = \mathbf{d}^{n+1}$$

The numerical experiments show that, in the case of low Reynolds numbers, this gives better results for the final velocity. However, it precludes the possibility to do the Guermond and Quartapelle's trick and eliminate the velocity correction step, as discussed earlier (see Equation (8)). We do not consider this scheme further.

Remark 2
The projection step can be further improved if instead of the 'preconditioner' used in Equation (26), $-(1+\hat{\hat{\sigma}})\nabla^2$, one follows the idea of Cahoet and Chabard [23] and use as a 'preconditioner' the (continuous) operator defined by its inverse: $\tau_0(1+\hat{\hat{\sigma}})^{-1}[1/Re - \tau_0(\nabla^2)^{-1}]$. This is equivalent to using a slightly compressible form of the continuity equation and leads to better results at low Reynolds numbers. However, it does not change the theoretical order of accuracy of the scheme and to make our analysis easier we do not consider it in the next sections. The expenses for such an approach are practically the same as for solving Equation (26) and therefore it should not be disregarded. Actually, it can be applied to the original (non-stabilized) incremental scheme *Splitting 1* with an LBB-compliant approximation, since it improves its result too at the same expenses.[3]

[3] Our numerical experiments using a problem with an exact solution showed decreases in the error at low Reynolds numbers but the convergence rate of the scheme was still second.

3. CHOICE OF THE STABILIZATION PARAMETER

3.1. Normal modes analysis

A question that still remains open is how to choose $\hat{\sigma}$ so that to retain the second-order temporal accuracy of the incremental projection scheme. In order to address this issue we consider the simplified one-dimensional flow model suggested by Orszag *et al*. [20] and used by E and Liu [6] in their analysis of several projection schemes. Fourier transform of the two-dimensional Stokes equations in one of the spatial directions (supposing periodic boundary conditions in this direction) yields the following set of one-dimensional boundary value problems:

$$\frac{\partial \mathbf{u}}{\partial t} + \nabla_k p = \nabla_k^2 \mathbf{u}$$

$$\nabla_k \mathbf{u} = 0$$

$$\mathbf{u}(\pm 1, t) = 0 \tag{28}$$

where k is the wave number of the Fourier transform and the differential operators subscripted by k are defined as

$$\nabla_k^2 \mathbf{u} = \left(\frac{\partial^2 \mathbf{u}}{\partial x^2} - k^2 \right), \qquad \nabla_k p = \begin{bmatrix} \partial p / \partial x \\ \mathrm{i}kp \end{bmatrix}, \qquad \nabla_k \cdot \mathbf{u} = \frac{\partial u}{\partial x} + \mathrm{i}kv \tag{29}$$

with u and v being the components of $\mathbf{u}$.

The *Stabilized Incremental Projection* as formulated above is difficult for a normal modes analysis and therefore we consider the Darcy form of a slightly different scheme

$$\tau_0 \mathbf{u}_*^{n+1} + \tau_1 \tilde{\mathbf{u}}^n + \tau_2 \tilde{\mathbf{u}}^{n-1} = -\nabla p^n + \frac{1}{Re} \nabla^2 \mathbf{u}_*^{n+1}, \quad \mathbf{u}_*^{n+1} = \mathbf{d}^{n+1}$$

$$\mathbf{u}_*^{n+1} - \mathbf{u}^{n+1} = \frac{1}{\tau_0} \nabla[(1 + \hat{\sigma}) p^{n+1} - p^n], \quad \nabla \cdot \mathbf{u}^{n+1} = 0$$

$$\mathbf{u}^{n+1} \cdot \mathbf{n}\big|_{\partial\Omega} = \mathbf{d}^{n+1} \cdot \mathbf{n} \tag{30}$$

Note that in the case of a Stokes flow, it yields the same PPE as in the *Stabilized Incremental Projection*. The velocity-correction step is different; however, this will not affect the main result of the normal mode analysis that follows. Orszag *et al.* [20] derived a normal mode solution of Equation (28) of the form

$$(\mathbf{u}, p)(x, t) = \mathrm{e}^{\gamma t}(\hat{\mathbf{u}}, \hat{p})(x) \tag{31}$$

with $(\hat{\mathbf{u}}, \hat{p})$ given by

$$\hat{u} = \cos(\mu x) - \cos(\mu)\frac{\cosh(kx)}{\cosh(k)}$$

$$\hat{v} = \frac{\mu}{\mathrm{i}k}\sin(\mu x) + \frac{1}{\mathrm{i}}\cos(\mu)\frac{\sinh(kx)}{\cosh(k)}$$

$$\hat{p}(x) = \frac{\gamma}{k}\cos(\mu)\frac{\sinh(kx)}{\cosh(k)} \tag{32}$$

in the symmetric case and by

$$\hat{u} = \sin(\mu x) - \sin(\mu)\frac{\sinh(kx)}{\sinh(k)}$$

$$\hat{v} = -\frac{\mu}{\mathrm{i}k}\cos(\mu x) + \frac{1}{\mathrm{i}}\sin(\mu)\frac{\cosh(kx)}{\sinh(k)}$$

$$\hat{p}(x) = \frac{\gamma}{k}\sin(\mu)\frac{\cosh(kx)}{\sinh(k)} \tag{33}$$

in the anti-symmetric case. The dispersion relation is specified by

$$\begin{cases} \mu\tan(\mu) + k\tanh(k) = 0 & \text{in the symmetric case} \\ \mu\cot(\mu) - k\coth(k) = 0 & \text{in the anti-symmetric case} \end{cases} \tag{34}$$

and

$$\gamma = -k^2 - \mu^2 \tag{35}$$

Scheme (30) applied to Equation (28) becomes[4]

$$\tau_0\mathbf{u}_*^{n+1} + \tau_1\mathbf{u}^n + \tau_2\mathbf{u}^{n-1} = -\nabla_k p^n + \nabla_k^2\mathbf{u}_*^{n+1}, \quad \mathbf{u}_*^{n+1}(\pm 1, t) = 0$$

$$\mathbf{u}_*^{n+1} - \mathbf{u}^{n+1} = \frac{1}{\tau_0}\nabla_k[(1+\hat{\sigma})p^{n+1} - p^n], \quad \mathbf{u}^{n+1}\cdot\mathbf{n}(\pm 1, t) = 0$$

$$\nabla_k\cdot\mathbf{u}^{n+1} = 0$$

[4] From now on we consider only the second-order version.

The semi-discrete normal modes then read

$$(\mathbf{u}^n, p^n) = l^n(\bar{\mathbf{u}}, \bar{p}), \qquad \mathbf{u}_*^{n+1} = l^{n+1}\bar{\mathbf{u}}^* \tag{36}$$

The set of equations can be integrated exactly and the solution (in the symmetric case) is given by

$$\bar{u} = \cos(\bar{\mu}x) - \cos(\bar{\mu})\frac{\cosh(kx)}{\cosh(k)}$$

$$\bar{v} = \frac{\bar{\mu}}{\mathrm{i}k}\sin(\bar{\mu}x) + \frac{1}{\mathrm{i}}\cos(\bar{\mu})\frac{\sinh(kx)}{\cosh(k)}$$

$$\bar{u}^* = \cos(\bar{\mu}x) - \cos(\bar{\mu})\frac{\cosh(kx)}{\cosh(k)} - \frac{\beta}{\tau_0}\bar{\delta}\cos(\bar{\mu})\left(\frac{\cos(\lambda x)}{\cos(\lambda)} - \frac{\cosh(kx)}{\cosh(k)}\right)$$

$$\bar{v}^* = \frac{\bar{\mu}}{\mathrm{i}k}\sin(\bar{\mu}x) + \frac{1}{\mathrm{i}}\cos(\bar{\mu})\frac{\sinh(kx)}{\cosh(k)} - \mathrm{i}k\frac{\beta}{\tau_0}\bar{\delta}\cos(\bar{\mu})\left(\frac{1}{\lambda}\frac{\sin(\lambda x)}{\cos(\lambda)} - \frac{1}{k}\frac{\sinh(kx)}{\cosh(k)}\right)$$

$$\bar{p}(x) = \beta(1+\bar{\delta})\cos(\bar{\mu})\left(\frac{1}{k}\frac{\sinh(kx)}{\cosh(k)} - \frac{1}{\lambda}\frac{\sin(\lambda x)}{\cos(\lambda)}\right) \tag{37}$$

with

$$\bar{\delta} = \frac{(1+\hat{\sigma})(2+\sqrt{1+2\beta\Delta t}) - 3 + 2\beta\Delta t}{(1+\hat{\sigma})(2+\sqrt{1+2\beta\Delta t})} \tag{38}$$

The dispersion relation is given by

$$\lambda^2 = -\tau_0\bar{\delta}^{-1} - k^2, \qquad \beta = -k^2 - \bar{\mu}^2$$

$$\bar{\mu}\tan(\bar{\mu}) - k\tanh(k) = \frac{\beta k\bar{\delta}}{\tau_0}\left(\tanh(k) - \frac{k}{\lambda}\tan(\lambda)\right) \tag{39}$$

The expressions for the anti-symmetric modes can be derived similarly to be

$$\bar{u} = \sin(\bar{\mu}x) - \sin(\bar{\mu})\frac{\sinh(kx)}{\sinh(k)}$$

$$\bar{v} = \frac{\bar{\mu}}{\mathrm{i}k}\cos(\bar{\mu}x) + \frac{1}{\mathrm{i}}\sin(\bar{\mu})\frac{\cosh(kx)}{\sinh(k)}$$

$$\bar{u}^* = \sin(\bar{\mu}x) - \sin(\bar{\mu})\frac{\sinh(kx)}{\sinh(k)} - \frac{\beta}{\tau_0}\bar{\delta}\sin(\bar{\mu})\left(\frac{\sin(\lambda x)}{\sin(\lambda)} - \frac{\sinh(kx)}{\sinh(k)}\right)$$

$$\bar{v}^* = \frac{\bar{\mu}}{\mathrm{i}k}\cos(\bar{\mu}x) + \frac{1}{\mathrm{i}}\sin(\bar{\mu})\frac{\cosh(kx)}{\sinh(k)} - \frac{\beta}{\tau_0}\bar{\delta}\sin(\bar{\mu})\left(\frac{1}{\lambda}\frac{\cos(\lambda x)}{\sin(\lambda)} - \frac{1}{k}\frac{\cosh(kx)}{\sinh(k)}\right)$$

$$\bar{p}(x) = \beta(1+\bar{\delta})\sin(\bar{\mu})\left(\frac{1}{k}\frac{\cosh(kx)}{\sinh(k)} - \frac{1}{\lambda}\frac{\cos(\lambda x)}{\sin(\lambda)}\right) \tag{40}$$

With the dispersion relation given by

$$\lambda^2 = -\tau_0\bar{\delta}^{-1} - k^2, \qquad \beta = -k^2 - \bar{\mu}^2$$

$$\bar{\mu}\cot(\bar{\mu}) - k\coth(k) = \frac{\beta k\bar{\delta}}{\tau_0}\left(\coth(k) - \frac{k}{\lambda}\coth(\lambda)\right) \tag{41}$$

From Equation (38) it is quite clear now that if $\hat{\delta}$ is chosen to be $O(\Delta t)$, $\bar{\delta}$ will be of the order of Δt and therefore the stabilized incremental scheme (in a Darcy form) will retain the second-order accuracy for the velocity of the original incremental scheme *Splitting 1*. It is also clear that the additional term in Equation (30) (compared with Equation (27)) is of the order of $(\Delta t)^2$ and therefore the present analysis as applicable to the original *Stabilized Incremental Projection*. Equations (39) and (41) show that the pressure will contain oscillations with magnitude and wavelength of order Δt.

We should emphasis here that this gives only the upper bound for the stabilization parameter. However, as discussed by Wathen and Silvester [24] in the case of stabilized Uzawa-like iteration, it cannot be chosen arbitrarily small. If $\hat{\delta}$ is below a certain value (which depends on the specific problem under consideration), the spurious pressure modes can reappear in the numerical solution. An estimate from below is discussed in the next subsection.

3.2. A stability bound for $\hat{\delta}$

Let us first introduce the following constants:

$$\theta^2(\mathbf{C}) = \min_{\mathbf{p}\in\tilde{\mathbf{P}}}\frac{\mathbf{p}^T\mathbf{C}\mathbf{p}}{\mathbf{p}^T\mathbf{M}_p\mathbf{p}} \tag{42}$$

$$\Theta^2(\mathbf{C}) = \min_{\mathbf{p}\in\tilde{\mathbf{P}}}\frac{\mathbf{p}^T\mathbf{C}\mathbf{p}}{\mathbf{p}^T\mathbf{M}_p\mathbf{p}} \tag{43}$$

where $\mathbf{M}_p$ is the standard pressure mass matrix, $\mathbf{C}$ is an arbitrary symmetric matrix of size M, $\tilde{\mathbf{P}}$ is $\mathscr{R}^M$ equipped with the norm induced by the pressure mass matrix and M is the number of the pressure degrees of freedom. Generally M is much greater than the number of velocity degrees of freedom N although the order of approximation for velocity and pressure is the same. Fortin and Pierre [25] have derived the following upper estimate for $\Theta(\mathbf{L}\mathbf{A}^{-1}\mathbf{L}^T)$ in the case of the generalized Stokes equations:

$$\Theta^2(\mathbf{L}\mathbf{A}^{-1}\mathbf{L}^T) \le n\frac{\Theta^2(\mathbf{S})}{\tau_0 + \nu\Theta^2(\mathbf{S})} \tag{44}$$

where n is the dimensionality of the physical space and $\nu = 1/Re$ (note that $\mathbf{S}$ is the discrete Laplacian on the velocity space). Then

$$\Theta^2(\mathbf{L}\mathbf{A}^{-1}\mathbf{L}^T + \hat{\sigma}\mathbf{S}_p) \leq n\frac{\Theta^2(\mathbf{S})}{\tau_0 + \nu\Theta^2(\mathbf{S})} + \hat{\sigma}\Theta^2(\mathbf{S}_p) \leq n\frac{\Theta^2(\mathbf{S}_p)}{\tau_0 + \nu\Theta^2(\mathbf{S}_p)} + \hat{\sigma}\Theta^2(\mathbf{S}_p) \tag{45}$$

A well-known inverse estimate is available for $\Theta(\mathbf{S}_p)$ provided that the grid is uniform (non-isoparametric), with an element size h (see, for example, Axelsson and Barker [26], pp. 235–238)

$$\Theta^2(\mathbf{S}_p) \leq \frac{c}{h^2} \tag{46}$$

c being independent of h.

An estimate from below for $\theta^2(\mathbf{L}\mathbf{A}^{-1}\mathbf{L}^T + \hat{\sigma}\mathbf{S}_p)$ is more difficult to obtain. Note that this would be a generalization of the LBB condition for the stabilized system. Maitre and Wabo [27] have derived such an estimate using the relation between the globally stabilized discretizations and the mini-element method, which uses locally introduced bubble functions for achieving stability. In our notations, their result (5.1) reads

$$\theta^2(\mathbf{L}\mathbf{A}^{-1}\mathbf{L}^T + \hat{\sigma}\mathbf{S}_p) \geq \min(1, m(\hat{\sigma}))\theta_s^2 \tag{47}$$

where θ_s is a stability constant of the LBB-stable mini-element and

$$m(\hat{\sigma}) = \min_k \frac{\hat{\sigma}|k||b_k|_{1,k}^2}{\left(\int_k b_k\right)^2} \tag{48}$$

Here k is an arbitrary element and $|k|$ is its measure.

Elementary considerations on a uniform (non-isoparametric) grid of size h show that

$$m(\hat{\sigma}) = \frac{d\hat{\sigma}}{h^2} \tag{49}$$

with the constant d being independent of h. Now, combining Equations (45), (46), (47) and (49) we can see that, for uniform grids, choosing $\hat{\sigma}$ to be of the order of h^2 will insure the stability of the stabilized system. Moreover, this choice makes the condition number of the stabilized Schur complement independent of the grid parameter h. Since $\hat{\hat{\sigma}} = \hat{\sigma}\tau_0$, this choice for $\hat{\sigma}$ gives

$$\hat{\hat{\sigma}} = O\left(\frac{h^2}{\Delta t}\right) \tag{50}$$

In the previous subsection we showed that accuracy considerations imply that $\hat{\tilde{\sigma}} = O(\Delta t)$. In practice, we usually choose Δt to be of the order of h and therefore these two estimates do not contradict to each other. Note that the stability restriction on the time step, induced by the method of characteristics, is given by $\Delta t \leq c_{\Delta t} h^{n/6}$.

It is quite difficult to evaluate the constants c and d in the general case. In the particular case, when the grid is constructed of cubes of size h sub-divided into five tetrahedra (see Figure 1) and in the case of $P_1 - P_1$ approximation, these constants are $c = 320$ and $d = 280$. If a higher-order polynomial approximation is used, the computation of d is quite complicated but the order of the stability constant in terms of h remains the same.

4. NUMERICAL RESULTS

In the present study we used mostly a $P_2 - P_2$ tetrahedral approximation. The reason was that in some cases (backward-facing step flow, for instance) the results with $P_1 - P_1$ approximation were quite inaccurate. The spatial integration was performed by means of a seventh-order Gaussian integration over a tetrahedron. The meshes that we used were produced by first splitting the numerical domain into cubes and then splitting each cube into five tetrahedra (see Figure 1). In all numerical experiments discussed in this chapter we performed the convection sub-step of any of the splitting schemes by means of the method of characteristics.

First we would like to discuss some results obtained with the usual incremental projection scheme *Splitting 1* for the driven cavity problem. The two-dimensional results of Guermond and Quartapelle [11], who used a $P_1 - P_1$ approximation (and a slightly different incremental projection, as discussed above), show that the pressure field at $Re = 100$ for $\Delta t = 0.1$ suffers of severe spurious oscillations. Our three-dimensional simulations in a cube, using both $P_1 - P_1$

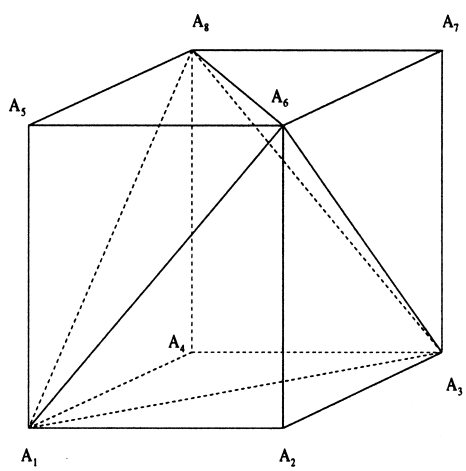

Figure 1. Sub-division of a cube into tetrahedra. The five tetrahedra are given by $A_1A_2A_3A_6$, $A_1A_6A_8A_5$, $A_1A_3A_8A_4$, $A_6A_3A_8A_7$ and $A_1A_3A_8A_6$.

and $P_2 - P_2$ approximations, produced a very reasonable, non-oscillatory result for the pressure field. In Figure 2 it is compared with the results obtained using an LBB-stable $P_2 - P_1$ tetrahedral approximation and of an iterative preconditioned Uzawa iteration technique for the generalized Stokes problem. In all the cases the convection step was performed by means of a characteristic method and the mesh contained 60921 nodes. This stable result seems to be due to the additional side wall boundary conditions in the three-dimensional cavity case.

However, the results with *Splitting 1* and both $P_2 - P_2$ and $P_1 - P_1$ approximations for the other benchmark problem, the backward-facing step flow suffered of severe node-to-node pressure oscillations, typical for the LBB-unstable discretizations (see Figure 3). Therefore, in the following we present mainly results with the *Stabilized Incremental Projection*. It is not surprising that the stability of the pressure calculations depends on the type of the problem

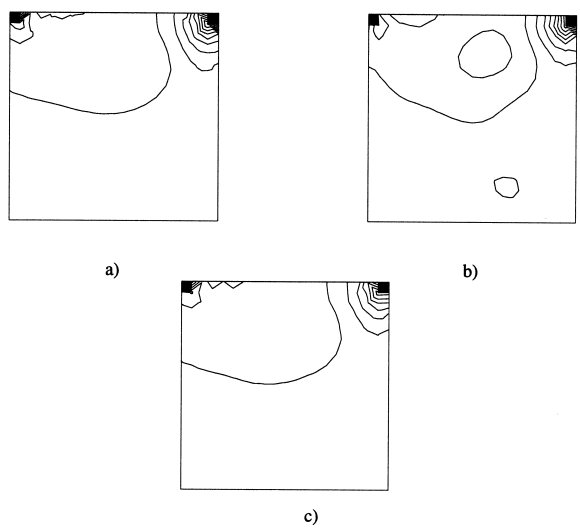

Figure 2. Steady state pressure contour lines for the flow in a driven cavity; $\Delta t = 0.1$, $Re = 100$. Results with *Splitting 1* and (a) LBB-stable $P_2 - P_1$ approximation; (b) $P_2 - P_2$ approximation. (c) shows the result with a preconditioned Uzawa iteration for the generalized Stokes problem and $P_2 - P_1$ approximation.

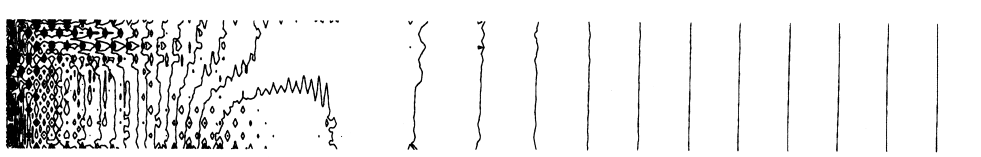

Figure 3. Pressure contour lines for the flow behind a backward-facing step; $Re = 200$, $\Delta t = 0.1$, $P_2 - P_2$ approximation with *Splitting 1*.

under considerations and that one can obtain reasonable (non-oscillatory) results with theoretically unstable elements (see for a discussion Brezzi and Fortin [29], p. 78).

The temporal convergence rate of the *Stabilized Incremental Projection* is first tested on the analytical solution used by Minev and Ethier [18]. The mesh in $\Omega = [-0.5, 0.5]^3$ contained 4401 nodes and 2560 elements. The stabilization parameter was set to $\hat{\tilde{\sigma}} = \Delta t$. The L_2 norm of the error for the velocity at different Reynolds numbers, measured at a fixed time $t = 0.8$, is presented in Table I. The increase of the error at $Re = 100$ and a very small time step is due to the influence of the characteristic scheme for the convection integration, which is known to exhibit such a behaviour (see Minev and Ethier [18]). Otherwise, the results for the velocity show a convergence rate very close to 2. The error in the pressure is presented in Table II. We should note here that no spurious oscillations are observed in the pressure results, although the time step, respectively $\hat{\tilde{\sigma}}$, is quite small in some of the experiments presented in Table II.

The *Stabilized Incremental Projection* is also benchmarked on the three-dimensional driven cavity problem. The parameters of the flow and mesh that were used are given above. The result for the profile of the horizontal velocity at the centreline of the cavity is compared with the numerical result of Iwatsu *et al.* [28] in Figure 4. In the same figure we also show the result of *Splitting 2* combined with a $P_2 - P_2$ approximation and homogeneous Neumann boundary conditions for the pressure. As already discussed, this scheme can suffer from large splitting errors, but since it is proportional to $1/Re$, we can expect that at large Reynolds numbers the result should be quite reasonable. Indeed, at $Re = 100$ all the results are quite close to each other, the maximum difference being less than 2 per cent. The pressure fields in both cases do not suffer spurious oscillations.

Finally, we present results for the flow behind a backward-facing step. As mentioned above, we obtained oscillatory pressure with *Splitting 1*. Although we solved the flow in three dimensions we imposed symmetry conditions in one of them so that the resulting flow mimics

Table I. L_2 norm of the velocity error at $t = 0.8$ for different time steps, Δt, and different Reynolds numbers.

Δt	$Re = 1$	$Re = 100$
0.1	0.006	0.0043
0.05	0.0016	0.00087
0.025	0.00042	0.00022
0.0125	0.00012	0.00024

Table II. L_2 norm of the pressure error at $t = 0.8$ for different time steps, Δt, and different Reynolds numbers.

Δt	$Re = 1$	$Re = 100$
0.1	0.35	0.086
0.05	0.1	0.016
0.025	0.039	0.0042
0.0125	0.033	0.014

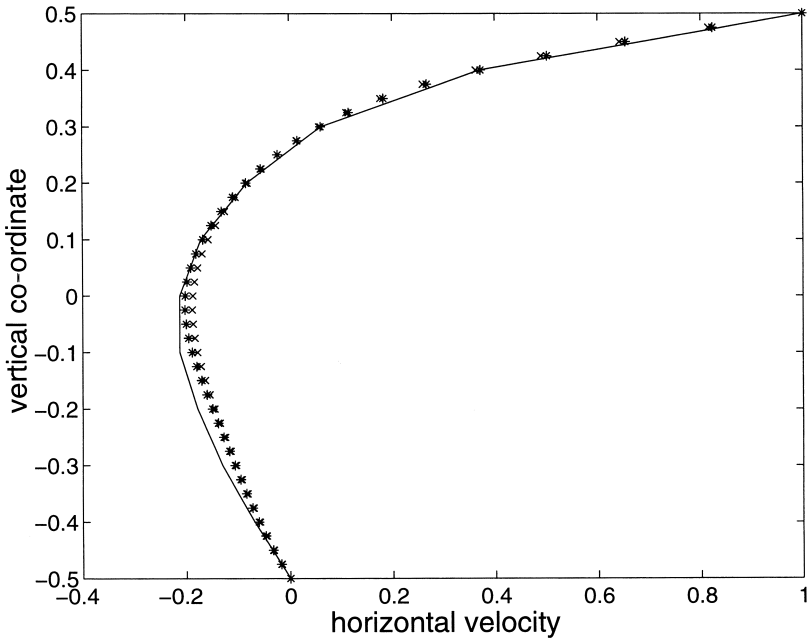

Figure 4. Steady state horizontal velocity profiles along the centreline of the cavity ($x = 0$, $y = 0$, $-0.5 \leq z \leq 0.5$) for lid-driven cavity flow at $Re = 100$. Solid line, results Iwatsu *et al.* [28]; results marked with *, *Stabilized Incremental Projection*; results marked with x, *Splitting 2* with $P_2 - P_2$ approximation and homogeneous Neumann condition for the pressure.

a two-dimensional one (at least for small Reynolds numbers). This enabled us to compare our results with several available experimental and numerical results for two-dimensional flow behind a step. The precise setting of the problem was the same as the one described by Minev and Ethier [18]. Initially we used a grid containing 22 525 and 11 800 tetrahedral elements in a 30-step heights long channel. The nodal spacing in the streamwise direction was 0.1 for the first ten step heights and then gradually increased to 0.2. In the other two directions the nodal spacing was 0.1. The problem was solved at $Re = 100$ and $Re = 200$ (the Reynolds number is based the height of the outlet), using time step $\Delta t = 0.2$ and $\Delta t = 0.1$ correspondingly. The *Stabilized Incremental Projection* with $P_2 - P_2$ tetrahedral approximation produced a non-oscillatory pressure field as can be seen in Figure 5, which presents the steady state pressure contour lines. For reference we also provide the contour lines obtained using the same characteristic integration of the convective terms but solving the generalized Stokes problem by means of a preconditioned Uzawa iteration technique (see Cahoet and Chabard [23]) and the result of *Splitting 1* with LBB-compliant $P_2 - P_1$ tetrahedra.

One of the most representative parameters of this flow is the length of the recirculation zone that is formed behind the step. The result obtained with the *Stabilized Incremental Projection* and $P_2 - P_2$ tetrahedra are compared with the result with *Splitting 1* with $P_2 - P_1$ tetrahedra and other available numerical and experimental data in Table III. The first two results are

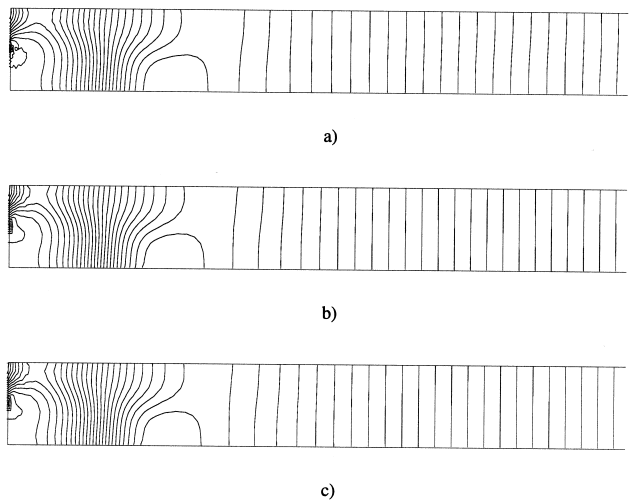

Figure 5. Steady state pressure contour lines for the flow behind a backward-facing step; $\Delta t = 0.1$, $Re = 200$. (a) shows results with *Stabilized Incremental Projection*; (b) *Splitting 1* and LBB-stable $P_2 - P_1$ approximation; (c) result with a preconditioned Uzawa iteration for the generalized Stokes problem.

Table III. Comparison of the dimensionless length of the recirculation zone for flow over backward-facing step, using the *Stabilized Incremental Projection* (SIP) and $P_2 - P_2$ tetrahedra, with the results of *Splitting 1* with $P_2 - P_1$ tetrahedra (S1), Timmermans *et al.* [12] (T) and Armaly *et al.* [31] (A).

Re	Numerical			Experimental
	SIP (3-D code)	S1 (3-D code)	T (2-D code)	A
100	3.16	3.23	3.2	3.2
200	5.26	5.29	5.4	–

quite similar and the slight underprediction of the recirculation length is due to insufficient spatial resolution rather than influence of the splitting error (Timmermans *et al.* use a high-order spectral element technique and a high-resolution grid in two dimensions).

The two-dimensional flow behind a step was very well documented by Gartling [30]. As it was noticed by this author, for $Re > 400$, the three-dimensionality of the flow becomes significant and the comparison of two-dimensional simulations with experimental data is unsatisfactory. In our case, although we imposed symmetry conditions on the front and back faces of the channel, we could not preclude the appearance of transversal waves. Therefore, we could not expect to obtain a very good comparison with two-dimensional results for $Re > 400$. We resolved the flow at $Re = 800$ using a variety of meshes and channel lengths. On the mesh of 22 525 elements (the channel length was 30 step heights) the length of the recirculation zone

of the lower wall eddy of the steady flow was about 11.4. Then, we used a uniform (and finer) grid of 112685 nodes and 60800 elements, the nodal spacing in streamwise and vertical direction being 0.05 and in transversal direction -0.1. On this grid we obtained a recirculation length of about 11.4 as well. The increase of the channel length to 40 step heights, keeping the same nodal spacing, did not significantly change the recirculation length and it was about 11.6. This is almost twice the two-dimensional value obtained by Gartling: 6.1. As could be expected, the value that we obtained is much closer to the experimental measurements of Armaly *et al*. [31]—about 14. In general, the precise resolution of this flow in three dimensions requires very expensive computations and it is beyond the scope of the present paper. More precisely, there are different three-dimensional flows of this type depending on the boundary conditions in the transversal direction. But it is quite clear from our results that they show the right trend of increase of the recirculation length.

5. CONCLUSIONS

The projection/splitting methods for the generalized Stokes problem can be considered as a first iteration of a preconditioned iterative procedure for inverting the Uzawa matrix with a particular initial guess and preconditioner. This helped us to derive a stabilized projection/splitting scheme from the classical globally stabilized Stokes system. It was then shown that the high-order splitting scheme proposed by Karniadakis *et al*. [16] can be considered as a particular case of this stabilized system for a specific choice of the stabilization parameter. Therefore it should yield stable pressure results (as confirmed by numerical experiments not presented here).[5] Unfortunately, the implementation of higher-order pressure boundary conditions is a relatively complicated procedure. Therefore we concentrated further on a globally stabilized incremental projection scheme. Using normal mode analysis and a simplified two-dimensional model flow we showed that if the stabilization parameter $\hat{\hat{\sigma}}$ is of order of Δt, then the stabilized scheme retains the second-order accuracy of the original incremental projection scheme. We also showed that the pressure stability is insured if $\hat{\hat{\sigma}} \geq d_\sigma h^2/\Delta t$. The theoretical order of accuracy of the scheme was verified numerically on a problem with an analytical solution and two benchmark problems. Our results are in a good agreement with other available numerical and experimental data. Moreover, the pressure does not contain spurious pressure oscillations. This was shown even for problems for which the non-stabilized scheme yielded node-to-node oscillations in the pressure field.

ACKNOWLEDGMENTS

The author would like to acknowledge the support of the National Science and Engineering Research Council (NSERC) of Canada via a research grant. He would also like to thank Phillip Gresho for encouraging him to study this problem.

[5] The same is true for the classical Chorin–Temam first-order scheme but in the present paper we focused mostly on the second-order schemes.

REFERENCES

1. Chorin AJ. Numerical solution of the Navier–Stokes equations. *Mathematics in Computers* 1968; **22**: 745–762.
2. Chorin AJ. On the convergence of discrete approximations to the Navier–Stokes equations. *Mathematics in Computers* 1969; **23**: 341–353.
3. Temam R. Une méthode d'aproximation de la solution des équations de Navier–Stokes. *Bulletin of the Society of Mathematics in France* 1968; **98**: 115–152.
4. Gresho P, Sani RL. *Incompressible Flow and the Finite Element Method*. Wiley: Chichester, 1998.
5. E W, Liu JG. Projection method I: convergence and numerical boundary layers. *SIAM Journal of Numerical Analysis* 1995; **32**: 1017–1057.
6. E W, Liu JG. Projection method II: Godunov–Ryabenki analysis. *SIAM Journal of Numerical Analysis* 1996; **33**: 1597–1621.
7. Bell JB, Colella P, Glaz HM. A second-order projection method for the incompressible Navier–Stokes equations. *Journal of Computational Physics* 1989; **85**: 257–283.
8. Kim J, Moin P. Application of a fractional-step method to incompressible Navier–Stokes equations. *Journal of Computational Physics* 1985; **59**: 308–323.
9. Guermond J-L, Quartapelle L. Calculation of incompressible viscous flows by an unconditionally stable projection FEM. *Journal of Computational Physics* 1997; **132**: 12–33.
10. Guermond J-L, Quartapelle L. On the approximation of the unsteady Navier–Stokes equations by finite element projection methods. *Numerische Mathematik* 1998; **80**: 207–238.
11. Guermond J-L, Quartapelle L. On incremental projection methods. In *Pitman Research Notes in Mathematics Series* (388), Salvi R (ed.). Longman: Essex, 1998; 277–288.
12. Timmermans LJP, Minev PD, van de Vosse FN. An approximate projection scheme for incompressible flow using spectral elements. *International Journal for Numerical Methods in Fluids* 1996; **22**: 673–688.
13. Minev PD, Ethier CR. A semi-implicit projection algorithm for the Navier–Stokes equations with application to flows in complex geometries. In *Notes on Numerical Fluid Mechanics* (73), Griebel M, Morgenov S, Yalamov P (eds). Vieweg: Braunschweig/Wiesbaden, 1999; 223–231.
14. Gresho P, Chan ST, Lee RL, Sani RL. A modified finite element method for solving the time-dependent, incompressible Navier–Stokes equations. Part 1: theory. *International Journal of Numerical Methods in Fluids* 1984a; **4**: 557–598.
15. Gresho P, Chan ST, Lee RL, Sani RL. A modified finite element method for solving the time-dependent, incompressible Navier–Stokes equations. Part 2: theory. *International Journal for Numerical Methods in Fluids* 1984b; **4**: 619–640.
16. Karniadakis GE, Israeli M, Orszag SA. High-order splitting methods for the incompressible Navier–Stokes equations. *Journal of Computational Physics* 1991; **97**: 414–443.
17. van Kan J. A second-order accurate pressure-correction scheme for viscous incompressible flows. *SIAM Journal of Scientific and Statistical Computing* 1986; **7**: 870–891.
18. Minev PD, Ethier CR. A characteristic/finite element algorithm using unstructured grids. *Computer Methods in Applied Mechanics and Engineering* 1999; **178**: 39–50.
19. Maday Y, Patera AT, Ronquist EM. An operator-integration-factor splitting method for time-dependent problems: application to incompressible fluid flow. *Journal of Scientific Computing* 1990; **5**: 263–291.
20. Orszag SA, Israeli M, Deville MO. Boundary conditions for incompressible flows. *Journal of Scientific Computers* 1986; **1**: 75–111.
21. Franca L, Hughes T, Stenberg R. Stabilized finite element methods. In *Incompressible Fluid Dynamics. Trends and Advances*, Gunzburger M, Nicolaides R (eds). Cambridge University Press: Cambridge, 1993; 87–107.
22. Axelsson O, Barker VA, Neytcheva M, Polman B. Solving the Stokes Problem on a Massively Parallel Computer. Report No. 9914, Department of Mathematics, University of Nijmegen [preprint], 1999.
23. Cahoet J, Chabard J-P. Some fast 3D finite element solvers for the generalized Stokes problem'. *International Journal for Numerical Methods in Fluids* 1988; **8**: 869–895.
24. Wathen A, Silvester D. Fast iterative solution of stabilized Stokes systems. Part I: using simple diagonal preconditioners. *SIAM Journal of Numerical Analysis* 1993; **30**: 630–649.
25. Fortin M, Pierre R. Stability analysis of discrete generalized Stokes problems. *Numerical Methods in Partial Differential Equations* 1992; **8**: 303–323.
26. Axelsson O, Barker VA. *Finite Element Solution of Boundary Value Problems: Theory and Computation*. Academic Press: New York, 1984.
27. Maitre JE, Wabo E. Stabilized formulations and mini-element for the n-dimensional Stokes equations: properties and solution procedure. In *Finite Element Methods: 50 years of the Courant Element*, Lecture Notes in Pure and Applied Mathematics (164), Križek M, Neittaanmäki P, Stenberg R (eds). Marcel Dekker: New York, 1994; 285–299.

28. Iwatsu R, Hyun JM, Kuwahara K. Analysis of three-dimensional flow calculations in a driven cavity. *Fluid Dynamics Research* 1990; **6**: 91–102.
29. Brezzi F, Fortin M. Mixed and hybrid finite element methods. In *Springer Series in Computational Mathematics* (15), Graham RL, Stoer J, Varga R (eds). Springer: New York, 1991.
30. Gartling DK. A test problem for outflow boundary conditions—flow over a backward-facing step. *International Journal for Numerical Methods in Fluids* 1990; **11**: 953–967.
31. Armaly BF, Durst F, Pereira JCF, Schönung A. Experimental and theoretical investigation of backward-facing step flow. *Journal of Fluid Mechanics* 1983; **127**: 473–497.

